

Solvation structure of the halides from x-ray absorption spectroscopy

Matthew Antalek,¹ Elisabetta Pace,² Britt Hedman,¹ Keith O. Hodgson,^{3,4}
 Giovanni Chillemi,^{5,a)} Maurizio Benfatto,^{2,b)} Ritimukta Sarangi,^{1,c)} and Patrick Frank^{1,3,d)}

¹Stanford Synchrotron Radiation Lightsource, SLAC National Accelerator Laboratory, Stanford University, Menlo Park, California 94025, USA

²Laboratori Nazionali di Frascati-INFN, P.O. Box 13, 00044 Frascati, Italy

³Department of Chemistry, Stanford University, Stanford, California 94305, USA

⁴SLAC National Accelerator Laboratory, Stanford University, Menlo Park, California 94025, USA

⁵CINECA, SCAI—SuperComputing Applications and Innovation Department, Via dei Tizii 6, 00185 Roma, Italy

(Received 16 March 2016; accepted 11 July 2016; published online 29 July 2016)

Three-dimensional models for the aqueous solvation structures of chloride, bromide, and iodide are reported. K-edge extended X-ray absorption fine structure (EXAFS) and Minuit X-ray absorption near edge (MXAN) analyses found well-defined single shell solvation spheres for bromide and iodide. However, dissolved chloride proved structurally distinct, with two solvation shells needed to explain its strikingly different X-ray absorption near edge structure (XANES) spectrum. Final solvation models were as follows: iodide, 8 water molecules at 3.60 ± 0.13 Å and bromide, 8 water molecules at 3.40 ± 0.14 Å, while chloride solvation included 7 water molecules at 3.15 ± 0.10 Å, and a second shell of 7 water molecules at 4.14 ± 0.30 Å. Each of the three derived solvation shells is approximately uniformly disposed about the halides, with no global asymmetry. Time-dependent density functional theory calculations simulating the chloride XANES spectra following from alternative solvation spheres revealed surprising sensitivity of the electronic state to 6-, 7-, or 8-coordination, implying a strongly bounded phase space for the correct structure during an MXAN fit. MXAN analysis further showed that the asymmetric solvation predicted from molecular dynamics simulations using halide polarization can play no significant part in bulk solvation. Classical molecular dynamics used to explore chloride solvation found a 7-water solvation shell at 3.12 ($-0.04/+0.3$) Å, supporting the experimental result. These experiments provide the first fully three-dimensional structures presenting to atomic resolution the aqueous solvation spheres of the larger halide ions. Published by AIP Publishing. [<http://dx.doi.org/10.1063/1.4959589>]

I. INTRODUCTION

The solvation structure of the halides, especially chloride, bromide, and iodide, remains under intense investigation, as recent reviews indicate.^{1–4} Ion solvation is an important subject of itself,⁵ but solvation structure also impacts, e.g., the dynamics of aqua-ion migration and electrode kinetics.⁶ Halide ion solvation governs the Hofmeister series defining protein salting-in and salting-out,^{7–10} while the immediate structure of dissolved halide influences the extended structure of water.^{11–13}

In pioneering work reported in 1973, Narten *et al.* used neutron and X-ray diffraction to examine the solvation structure of chloride.¹⁴ This and subsequent neutron and X-ray determinations of halide solvation revealed approximately 6-fold (octahedral) solvation, with X–O distances (X = Cl[−], Br[−], and I[−]) of 3.3 Å, 3.4 Å, and 3.7 Å, respectively.¹⁵

In all cases, solvating water molecules were found oriented so as to each produce a single HO–H ··· X[−] hydrogen bond. Later studies, also including anomalous X-ray diffraction (AXD) and extended X-ray absorption fine structure (EXAFS) analyses have generally confirmed the earlier results.^{2,4,16–28} However, these room temperature studies have a large error in the first shell determination. For example at room temperature, the EXAFS structural approach, although extremely powerful, has an estimation accuracy of $\pm 25\%$ in coordination number (CN) and ± 0.03 Å in bond length,^{29,30} indicating that the consensus halides solvation structure derived from EXAFS is actually $CN = 6 \pm 2$.

Molecular dynamics (MD) modeling has successfully reproduced observables relevant to the structure and dynamics of liquid water, such as O–O and O–H scattering profiles and proton exchange.^{2,14,23,31–34} Likewise, MD has been used extensively to predict the solvation of the halides.^{12,33–40} MD simulations explicitly including halide polarizability have predicted a highly asymmetric solvation environment.^{8,38,41–46} However, other MD simulations did not find asymmetric solvation,^{21,33,47–50} and MD combined with density functional theory (DFT) apparently gives mixed results regarding the symmetry of halide solvation.^{21,22,35,36,51–55} For example DFT/MD has been found to be superior to,^{21,35} or less accurate than,⁵⁴ classical MD. The error in basis set superposition

a)Email: g.chillemi@cineca.it. Tel.: +39 06 44486 706. Fax: +39 051 2130225.

b)Email: Maurizio.Benfatto@lnf.infn.it. Tel.: +39-06-9403-2884. Fax: +39-06-9403-2582.

c)Email: ritis@slac.stanford.edu. Tel.: +1-650-926-4621. Fax: +1-650-926-4100.

d)Author to whom correspondence should be addressed. Electronic mail: pfrank@slac.stanford.edu. Tel.: +1-650-723-2479. Fax: +1-650-723-4817.

energy (BSSE) can limit the accuracy of DFT/MD simulations.⁵⁵ MD also predicts that anion polarizability causes the heavier halides to preferentially migrate to the surface of a water-air interface ($\text{Cl}^- < \text{Br}^- \ll \text{I}^-$).^{7,8,38,41,45} Experimental support for this effect has been reported.^{56–59}

Minuit X-ray absorption near-edge (MXAN) analysis has emerged as a powerful method of deriving local structure from x-ray absorption spectroscopy (XAS) spectra.^{60–63} MXAN uses extended continuum multiple scattering (ECMS) theory to iteratively fit the entire XAS spectrum, using an input structural model that is relaxed during the course of the fit. MXAN fits yield both distance (± 0.02 Å) and angle ($\pm 2^\circ$) information, thereby providing three-dimensional local structures that best reproduce the experimental spectra. MXAN fits take explicit account of both the low-lying bound-state transitions of the X-ray absorption near edge structure (XANES) energy region and the long-range multiple-scattering. MXAN analysis is especially powerful for room temperature data because the XANES is not significantly affected by structural disorder.^{64–66}

The strengths of EXAFS and MXAN analysis can be combined to allow rapid derivation of likely structural models (EXAFS) that can be tested and refined (MXAN). For example combined EXAFS and MXAN analysis revised the long-held view that aqueous dissolved Cu(II) complex ions, including the aqua-ion, inhabit a six-coordinate Jahn-Teller distorted octahedron. Instead, an axially elongated five-coordinate square pyramid dominates, which however includes a ~ 3 Å non-bonded axially solvating water molecule.^{67–70}

Herein we report the full XAS analysis using combined MXAN and EXAFS to derive the structure of dissolved aqueous chloride, bromide, and iodide ions. MD analysis was then carried out to derive the dynamical behavior of chloride ion in light of these models. Finally, density functional theory (DFT) was used to evaluate the electronic consequences of the structural models.

II. MATERIALS AND METHODS

Sodium chloride (NaCl), rubidium bromide (RbBr), and potassium iodide (KI) were purchased from Aldrich Chemicals and used without further purification. All solutions were prepared in doubly deionized (18 MΩ) water.

X-ray absorption spectra were measured at the Stanford Synchrotron Radiation Lightsource (SSRL). Soft X-ray beamline 4-3 was employed to measure the chloride K-edge XAS spectra of aqueous NaCl or the iodide L₁-edge of aqueous KI under standard ring conditions (3 GeV, 500 mA) in the fluorescence mode using the PIPS silicon-drift detector. The bromide K-edge of aqueous RbBr was measured using a 13-element Ge-detector at SSRL beamline 10-2 (3 GeV, 300 mA) operating in unfocussed mode and 50% detuned at 13 keV to reject higher harmonics. Samples were in ambient temperature aqueous solution, held in 2 mm path length Teflon spacer cells faced with 5 μm polypropylene windows.

XAS spectra were calibrated at the energy of the first inflection on the rising edge (chloride, 2833.0 eV; bromide, 13474.0 eV, and; iodide, 5188.0 eV). XAS spectra presented here are the average of several individual scans.

The raw spectra were processed and normalized as has been described previously.^{71,72} Normalization was carried out using the application Pyspline.^{69,73} EXAFS spectra were fit using the Feff8 code within the program suite EXAFSPAK,^{30,74,75} <http://www-ssrl.slac.stanford.edu/~george/exafspak/exafs.htm>. EXAFS goodness-of-fit is determined as

$$\text{Weighted } F = \left[\sum k^6 (\chi_{\text{exp}} - \chi_{\text{calc}})^2 / \sum k^6 \chi_{\text{exp}}^2 \right]^{1/2}. \quad (1)$$

Coordination numbers (CN) were integer-stepped. Bond distance (R) and mean displacement (σ^2) were varied independently for each scattering path. Energy shift (ΔE_0) was varied but linked among the paths. The expected fit resolution between shells for each halide was 0.22–0.26 Å, calculated as $\pi/2\Delta k$, where Δk is the fitted k -range in Å^{−1}. Actual resolution of the EXAFS is likely much better than this, because the functional form of EXAFS is well-understood.⁷⁶ Solvation shell distances were initially surveyed by varying X–O distance step-wise with the coordination number (CN) fixed at 1.0, while σ^2 and ΔE_0 were floated (X = Cl[−], Br[−], I[−]). For coordination number searches, CN was varied step-wise while X–O distance, σ^2 , and ΔE_0 were floated. In the final fits, precision in X–O distance is reported as the 1σ numerically estimated standard deviation (e.s.d.). The reported EXAFS Fourier transforms were uncorrected for phase shift. The EXAFS scale factor (S_0^2) was fixed at one following its evaluation through a series of fits (see Table S1 in the supplementary material).¹²⁸

MXAN fits were carried out over an energy range 150 eV (chloride, bromide) or 125 eV (iodide) above E_0 . MXAN energy was expressed in the E- E_0 scale, where $E_0 = 2834.62$ eV (Cl[−] K-edge), 13473.52 eV (Br[−] K-edge), or 5189.0 eV (I[−] L₁-edge). The MXAN method and extended continuum multiple scattering (ECMS) theory have already been described in detail.^{61,62,77,78} The function minimized during the MXAN fit was defined as

$$R_{sq} = n \frac{\sum_{i=1}^m w_i \left[(y_i^{\text{th}} - y_i^{\text{exp}}) \varepsilon_i^{-1} \right]^2}{\sum_{i=1}^m w_i}, \quad (2)$$

where “ n ” is the number of independent parameters, “ m ” is the number of data points, “ y_i^{th} ” and “ y_i^{exp} ” are the theoretical and experimental values of the absorption, respectively, “ ε_i ” is the error in each point of the experimental data set, and the statistical weight “ w_i ” = 1. The experimental error ε_i is a constant 1.0% of the main experimental edge jump over the whole data set.

Atomic coordinates for the Feff and MXAN input files were derived from structural models constructed within the program Chem 3D Pro or ChemBio 3D Ultra 14.0 (CambridgeSoft Corp.). Precision in MXAN bond-length is reported as the 1σ fit standard deviation.

EXAFS fits were evaluated using the statistical criteria of Michalowicz *et al.*⁷⁹

$$F_M = (\chi_1^2/\nu_1)/(\chi_2^2/\nu_2), \quad (3)$$

where $\Delta \chi_n^2$ is the chi-squared value of fit “ n ,” $\nu_n = N_{\text{ind}} - N_{\text{par}}$ is the degrees of freedom in the fit, N_{ind} is the number of

independent data points, and N_{par} is the number of adjustable parameters. The N_{ind} was calculated using the Stern equation, $N_{\text{ind}} = (2 \times \Delta R \Delta k / \pi) + 2$.⁸⁰ The condition $F_M > 1$ determines the statistically valid choice between the competing models.⁸¹

When the number of degrees of freedom changes between fits ($\nu_2 < \nu_1$ and $\chi^2_2 < \chi^2_1$), then Eq. (4) is preferred,

$$F_M = [(\Delta\chi^2_1 - \Delta\chi^2_2)/(\nu_1 - \nu_2)]/(\Delta\chi^2_2/\nu_2). \quad (4)$$

A. Density functional theory

Gradient-corrected generalized gradient approximation (GGA), spin-restricted, broken-symmetry density functional calculations were carried out using the ORCA package. The hybrid B3LYP functional was employed to hydrogen optimize the 6-, 7-, and 8- coordinate structures obtained after MXAN fits to the XAS data. A conductor like screening model (COSMO) was chosen to simulate the water solvation. TightSCF convergence criterion was chosen. The Ahlrichs' all electron triple- ζ TZVPP basis set was used on all atoms. Time-dependent density functional theory (TD-DFT) calculations were performed from Cl 1s to valence levels employing both the dipole and quadrupole operators. The `orca_mapspc` script was used to generate simulated spectra.

B. Molecular dynamics

Molecular Dynamics (MD) simulations and analysis of chloride solvation were all carried out with the Gromacs package, version 4.6.5.⁸² The simulated system was composed of one Cl ion and 1077 bulk water molecules, using either SPC/E,⁸³ TIP3P,⁸⁴ or TIP5P⁸⁵ force fields. After energy minimization, the systems were equilibrated for 5 ns followed by production simulation in the NVT ensemble carried out for 50 ns. The simulation time step was 1 fs, and frames were extracted every 1 ps. The particle-mesh Ewald method was used for the treatment of the long-range electrostatic interactions,⁸⁶ while V-rescale temperature coupling was employed to maintain the temperature at 300 K.⁸⁷

The instantaneous MD snapshot geometries were used to obtain MXAN simulated XAS spectra and averaged to obtain the so-called dynamic MXAN or D-MXAN spectrum. For individual D-MXAN calculations, the structural parameters were fixed, while the non-structural parameters were floated. The Reif and Hünenberger L_E , M_E , and H_E , and the Gromos

version 54A Lennard-Jones parameters for the Cl-water interaction were tested.^{88,89} The Gromos parameters were also tested using the Gromacs Encad-shift option, which decreases the Coulomb potential throughout the range.⁹⁰

Further refinements were made by selecting MD frames using the error-minimization function R_{th} , defined as

$$R_{\text{th}} = \frac{\sqrt{\sum_{i=1}^m (\sigma_i^{\text{MD}} - \sigma_i^{\text{th}})^2}}{m}, \quad (5)$$

where m is the total number of theoretical energy points, σ_i^{MD} is the cross section at the i th energy point for a given MD snapshot, and σ_i^{th} is the MXAN-theoretical cross section at the same energy point obtained using the geometrical structure at the solution-phase best fit. The criterion for acceptance of a frame was $R_{\text{th}} < 7 \times 10^{-4}$.

III. RESULTS

Figure 1 compares the XAS spectra and the first derivatives of the XAS spectra of chloride, bromide, and iodide, all plotted on a common E- E_0 energy scale. Immediately apparent is that bromide and iodide produce very similar XANES spectra, while chloride is unique. Part of the similarity of the bromide and iodide spectra resides in core-hole lifetime broadening (bromide $K = 2.52$ eV, iodide $L_1 = 3.46$ eV),⁹¹ which reduces spectral resolution. Nevertheless, dissolved chloride produces XANES features that are clearly absent from the spectra of the other two halides. The three halide ions are all filled shell and homologically iso-electronic ($3p^6$, $4p^6$, $5p^6$). Therefore, the distinctive chloride features do not arise from an inequivalent ground state electronic configuration relative to the other halides. These differences will find an explanation in the analysis below.

The dramatic difference in the near-edge data between chloride and the higher halides is also manifested in the EXAFS region. A superposition of the FT spectra (calculated over the same EXAFS region of $k = 2-8 \text{ \AA}^{-1}$) shows a significantly broader first shell in Cl relative to the higher halides, suggesting a more extended coordination sphere (Figure S1-1 in the supplementary material).¹²⁸ This hypothesis is tested using FEFF-8 fits to the EXAFS data, shown below.

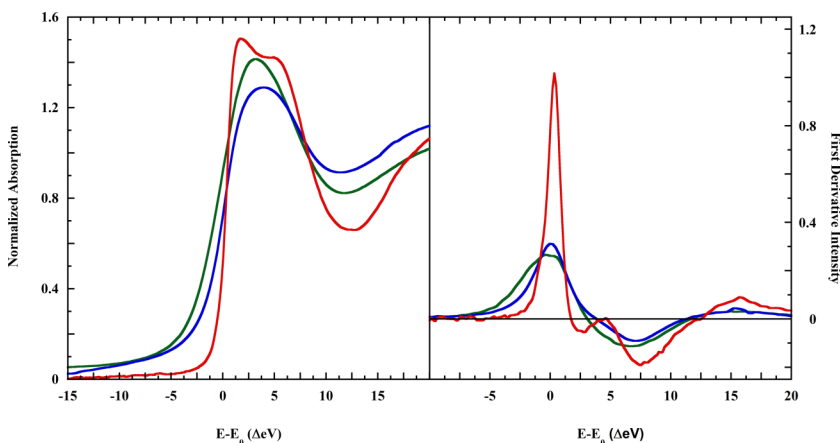


FIG. 1. Normalized, ambient-temperature XANES and their corresponding first derivative spectra for the following: (red solid line), NaCl (40 mM, Cl^- K-edge); (green solid line), RbBr (0.5 M, Br^- K-edge); and (blue solid line), KI (25 mM, I^- L_1 -edge). The XAS spectra are plotted on a common E- E_0 energy scale (see Sec. II for E_0 values).

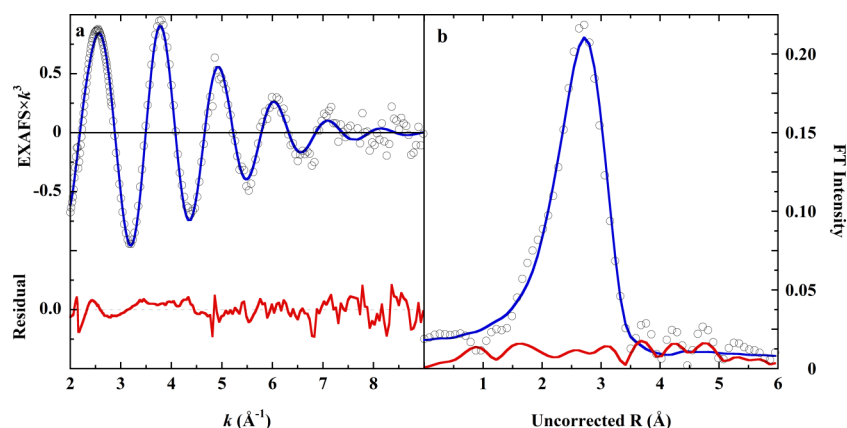


FIG. 2. (a) (Open circle), EXAFS spectrum of KI in water solution; (blue solid line), the fit with nine oxygen scatterers at 3.50 Å; and (red solid line), the unfit residual. Panel (b). The Fourier transform spectrum of the EXAFS and the fit.

In the remainder of this paper, the solvation structures of the halides are first assessed using EXAFS and MXAN analysis. In each case, a three-dimensional model is derived. MXAN fits are computationally more expensive and more protracted than EXAFS fits. Therefore, EXAFS analytical models can be used to quickly reduce the structural phase space to be explored by subsequent MXAN analysis. The MXAN fit to the XAS of dissolved chloride is then compared with the result from the D-MXAN analysis using the classical MD framework. Finally, time-dependent density functional theory (TD-DFT) is used to evaluate the electronic state of solvated chloride.

A. Iodide

1. EXAFS analysis

Figure 2 shows the L_1 -edge EXAFS spectrum of iodide in water, the fit (see below), and the corresponding Fourier transform spectra. The EXAFS attenuates rapidly, with little intensity beyond $k = 8 \text{ Å}^{-1}$. This behavior was also found by others^{21,27,53,54} and is a characteristic of the EXAFS of the other halides as well.^{20,35,53,54} Hydrogens were not included in the fits because this short EXAFS range limited the number of statistically independent data points. The preliminary search of weighted F-value over I–O distances of range 2.5–4.5 Å produced a single deep minimum at 3.50 Å. A similar search over coordination number (CN) yielded a broad minimum centered at CN = 9 (Figure S1-2 of the supplementary material).¹²⁸ The full fit using a single shell of nine oxygen scatterers (weighted F = 0.1641) indeed proved better than either eight (weighted F = 0.1777) or ten (weighted F = 0.1701) scatterers.

Although the best fits overall were obtained using three shells of oxygen scatterers, the Michalowicz criterion

eliminated all the models competing with the single-shell CN = 9 fit presented in Figure 2 and Table I.

The EXAFS $\pm 25\%$ resolution in coordination number implies a best estimate of CN = 9 ± 2 water molecules for the iodide solvation sphere.

The large σ^2 value in the CN = 9 fit implies radial disorder among the I–O distances, which is not reflected in the small statistical error, but potentially lowers the reliability of the first shell coordination number.

2. MXAN analysis

MXAN analysis includes both the XANES and the continuum parts of an XAS spectrum, thus evaluating a distinctly different data set than does an EXAFS analysis. In particular, the symmetry-dependent intensities of the bound state transitions in the XANES part of the XAS spectrum constrain the angular arrangement of the scattering atoms surrounding the absorber. MXAN fits were used to test iodide solvation spheres of 4, 6, 8, and 10 waters. Hydrogens were included in the models, and the waters were always arranged to present a single H-bond to iodide, consistent with

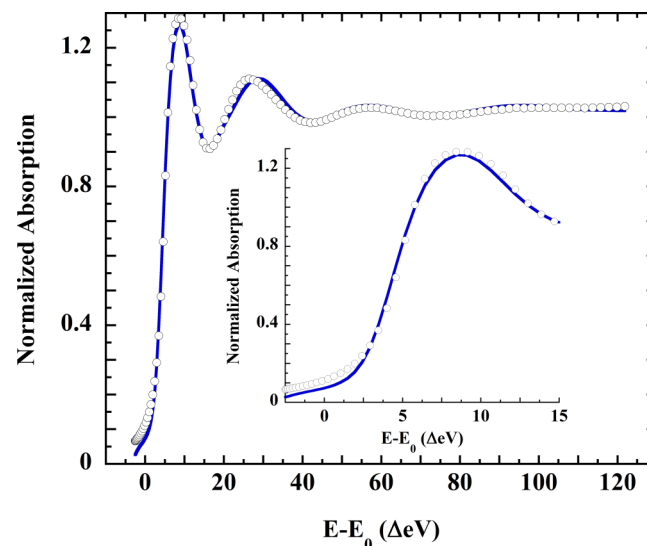


FIG. 3. (Open circle), L_1 -edge XAS spectrum of potassium iodide in water and (blue solid line), the MXAN fit with an 8-water solvation sphere; $R_{sq} = 2.38$. Inset: the rising edge energy region.

TABLE I. EXAFS metrics for the iodide solvation sphere.

	[CN] R (Å) ^a	$\sigma^2 \times 10^3$	ΔE_0 (eV)	Weighted F
I–O	[9] 3.50 ± 0.003	34.840	−0.4598	0.1641

^aCN is the coordination number. Uncertainty is the fit statistical e.s.d; empirical uncertainty for room temperature solution EXAFS is of order $\pm 0.03 \text{ Å}$. The σ^2 is in units of Å^2 .

TABLE II. MXAN best fit metrics for the iodide solvation sphere.

Model	I–O (Å) ^{a,b}	I–H _{near} (Å) ^a	I–H _{far} (Å) ^a	R _{sq}
6-waters	3.40 ± 0.09	2.48 ± 0.14	3.90 ± 0.18	5.18
8-waters	3.59 ± 0.13	2.67 ± 0.21	4.08 ± 0.25	2.38
10-waters	3.65 ± 0.18	2.69 ± 0.18	4.05 ± 0.18	12.94
Prior work				
CN ^c	I–O (Å) ^a	I–H _{near} (Å) ^a	Method ^d	References
6	3.5	2.7	EXAFS and XANES	25
6	3.60	2.65 (est.)	XRD	92
7	4.11 ± 0.20	3.27 ± 0.16	ND	93
6	3.50 ± 0.03	2.65 ± 0.03	EXAFS	21

^aBond lengths include ±1σ scatter in I–L distance; L = O, H.^bThe I–O distance RMS ± (fit-error) ± (error standard deviation) was: 6-water model, ±0.05 ± 0.01 Å; 8-water model, ±0.21 ± 0.15 Å; 10-water model, ±0.06 ± 0.08 Å.^cIn D₂O.^dEXAFS, extended X-ray absorption fine structure; XANES, X-ray absorption near-edge spectrum; XRD, X-ray diffraction; ND, neutron diffraction.

the configuration implied by X-ray and neutron scattering experiments.^{2,14,23,34}

These fits produced goodness-of-fit values, R_{sq} = 10.83, 5.18, 2.38, and 12.94, respectively. The best fit 8-water solvation sphere is shown in Figure 3. The fit metrics for 6, 8, and 10 waters appear in Table II, along with results from previous studies.

The structural model arising from this fit features water molecules in a 2, 4, 2 configuration and is displayed in Figure 9(a). The average MXAN I–O distance of 3.59 ± 0.13 Å (range 3.37–3.80 Å) compares favorably with the average EXAFS distance of 3.50 ± 0.03 Å. The spread of I–O distances in the MXAN fit, combined with the lack of a direct I–O bond and room temperature measurement, provides a physical explanation for the large σ² in the EXAFS model noted above. As implied from EXAFS analysis, the fitted set of I–O distances obtained from XANES analysis should be seen as the equilibrium average ground state structure within a dynamic process, rather than as only one of many instantaneous structures. The 8-coordinate fit is entirely consistent with the prior 6-coordinate EXAFS fits reported by others (Table II), which likewise have a 25% uncertainty in coordination number.

B. Bromide

1. EXAFS analysis

EXAFS analysis in Figure 4 shows the bromide K-edge spectrum of RbBr in water solution, the fit, and the corresponding Fourier transform spectrum. As with iodide, the EXAFS attenuates rapidly, with little intensity beyond $k = 9 \text{ Å}^{-1}$.

A survey of Br–O distance within a 2.5–4.5 Å range showed one EXAFS goodness-of-fit minimum at 3.28 Å, implying a single solvation sphere. Br–O coordination numbers surveyed between one through fourteen found a broad minimum at CN = 10. These results are shown in Figure S2-1 of the supplementary material.¹²⁸ The EXAFS CN = 10 best fit (weighted F = 0.1524) yielded Br–O = 3.26 Å. Splitting the 10-water shell into two CN = 5 shells did not improve the fit (weighted F = 0.1607), and the Δ_{shell} = 0.06 Å was far below the resolution limit. The CN = 11 fit was nearly as good (weighted F-value = 0.1568, F_M = 1.06, Br–O = 3.26 Å) and cannot be excluded with certainty. The single shell CN = 10 fit is shown in Figure 4. Table III presents the fit metrics. As before, the limit of EXAFS resolution implies the solvation CN = 10 ± 3. The rather large σ² value again

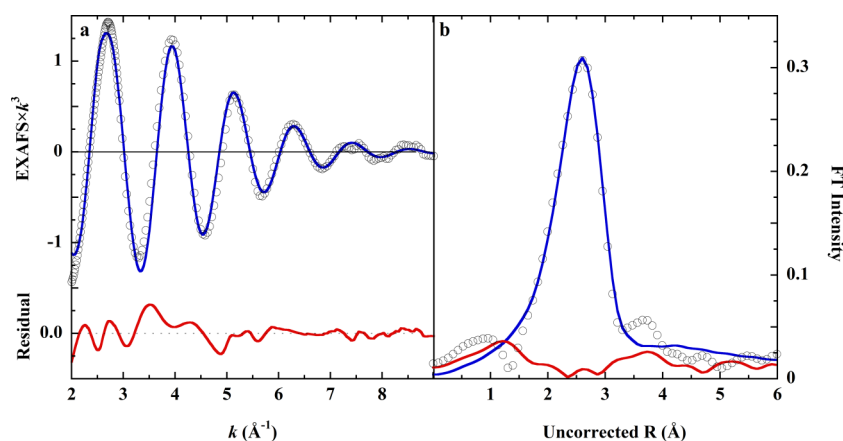


FIG. 4. (a) (Open circle), EXAFS spectrum of RbBr in aqueous solution; (blue solid line), the fit with 10 oxygen scatterers at 3.28 Å; and (red solid line), the unfit residual. Panel (b). The Fourier transform spectrum of the EXAFS and the fit.

TABLE III. EXAFS metrics for the bromide solvation sphere.

	(CN) R (Å) ^a	$\sigma^2 \times 10^3$	ΔE_0 (eV)	Weighted F
Br-O	[10] 3.26 ± 0.003	34.520	0.0599	0.1524

^aCN is the coordination number. Uncertainty is the fit statistical e.s.d; empirical uncertainty for room temperature solution EXAFS is of order ± 0.03 Å. The σ^2 is in units of Å².

implies a radially disordered solvation sphere and can further limit the resolution of coordination number.

When the EXAFS fit coordination number was restricted to 6.0 or 7.0, the Br-O distance was 3.33 ± 0.1 Å or 3.30 ± 0.01 Å, respectively, consistent with previous EXAFS studies employing models of equivalent CN.^{18,19,28} However, the poorer goodness-of fit weighted F-values, 0.3435 and 0.2530, and the distinctly lower quality of these fits eliminated the CN = 6 and CN = 7 models from further consideration.

2. MXAN analysis

MXAN fits to the bromide XAS spectrum was used to explore solvation spheres of four ($R_{sq} = 4.86$), six ($R_{sq} = 3.24$), seven ($R_{sq} = 2.35$), eight ($R_{sq} = 2.24$), and ten ($R_{sq} = 1.93$) water molecules. These fits are compared in Figures S2-2 and S2-3 in the supplementary material.¹²⁸ The improved quality in the CN = 7 fit relative the CN = 6 is visually apparent (Figure S2-2). Figure S2-3 displays the CN = 6 and CN = 7 structural models differentiated by the fit R_{sq} values, demonstrating the ability of MXAN analysis to discern between solvation spheres distinguished by a single water molecule. On the other hand, the quality of the CN = 7, CN = 8, and CN = 10 fits proved highly similar, cf. Figure S2-3, despite variation among the models by up to three water molecules.

However in the CN = 10 fit, one of the water molecules migrated out to Br-O = 4.41 Å. This is the extreme limit of allowed outward migration within the MXAN routine, implying attempted rejection of that water molecule. Two of the remaining nine water molecules had moved to an H₂O...H-OH distance of 1.3 Å, which is excessively short.⁹⁴⁻⁹⁷ These results provided grounds to set aside the CN = 10 model.

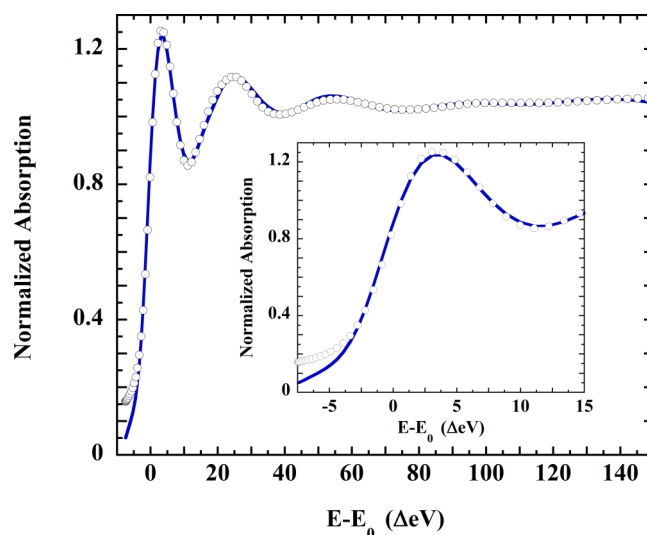


FIG. 5. (Open circle), K-edge XAS spectrum of rubidium bromide in water and (blue solid line), the MXAN fit with an 8-water solvation sphere; $R_{sq} = 2.24$. Inset: the rising edge energy region. See Figure 9(b) for the structure producing this fit.

The remaining CN = 7 and CN = 8 models are statistically indistinguishable and can be usefully compared as an approximate square plane of four waters, with 2 + 1 (CN = 7) or 2 + 2 (CN = 8) axially disposed water molecules. Table IV compares the metrics of these models.

Figure 5 shows the fit to the bromide K-edge spectrum produced by CN = 8 model. The CN = 7 fit is shown in Figure S2-3 in the supplementary material.¹²⁸ Figure 9(b) displays the structural model corresponding to the CN = 8 fit, and the CN = 7 structural model is shown in Figure S2-4 in the supplementary material.¹²⁸

Both sets of model metrics are completely consistent with other experimentally determined Br-O distances for dissolved aqueous bromide.^{2,19,22,24,26,28,98} These structures can equally represent dissolved bromide and are nearly interconvertible through a single water molecule. They are thus consistent with equilibrium partners in the dynamics of bromide solvation in water. In that sense, they are comparable with the fractional solvation populations recently deduced by Migliorati *et al.*⁵³

TABLE IV. MXAN best fit metrics for the two equivalent bromide solvation spheres.

Model	Br-O (Å) ^{a,b}	Br-H _{near} (Å) ^a	Br-H _{far} (Å) ^a	R_{sq}
7-waters	3.41 ± 0.12	2.54 ± 0.23	3.82 ± 0.14	2.35
8-waters	3.40 ± 0.14	2.48 ± 0.22	3.88 ± 0.22	2.24
Prior work				
CN ^c	Br-O (Å) ^a	Br-H _{near} (Å) ^a	Method ^d	References
6	3.19	...	EXAFS	26
6.9	3.34	...	EXAFS	18
6	3.2	...	EXAFS	28
7 ± 1	3.4	...	AXD	24
6 ± 0.5	3.44 ± 0.07	...	EXAFS	22

^aBond lengths include $\pm 1\sigma$ scatter in Br-L distance; L = O, H.

^bThe Br-O distance RMS \pm (fit-error) \pm (error standard deviation) was: 7-water model, $\pm 0.40 \pm 0.23$ Å; 8-water model, $\pm 0.46 \pm 0.19$ Å; 10-water model, $\pm 0.31 \pm 0.28$ Å.

^cCoordination number.

^dEXAFS, extended X-ray absorption fine structure; AXD, anomalous X-ray diffraction.

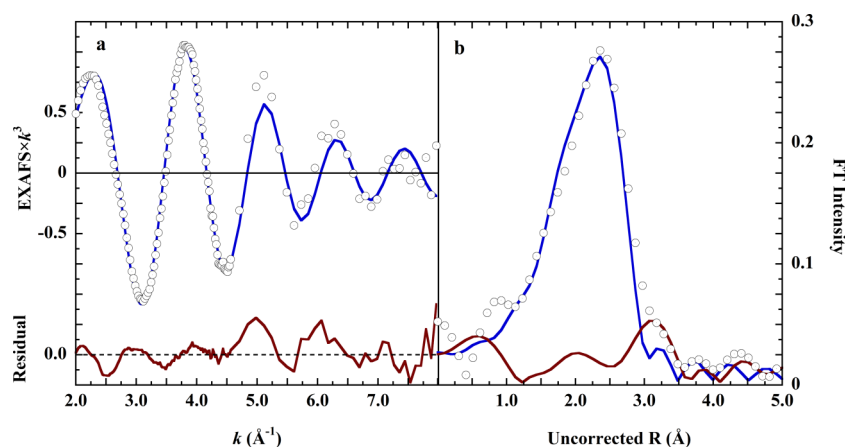


FIG. 6. (a) (Open circle), K-edge EXAFS spectrum of chloride in water; (blue solid line), fit with a split shell totaling seven oxygen scatterers; and (red solid line), unfit residual. (b) Fourier transform of the following: (open circle), the EXAFS data, (blue solid line), the fit, and (red solid line), the unfit residual. See the text for details.

C. Chloride

1. EXAFS analysis

EXAFS of dissolved chloride, shown in Figure 6, again displayed the rapid attenuation of signal intensity typical of the heavier halides. For chloride, the exploration of goodness-of-fit vs. distance produced three distinct Cl–O distance minima, at 2.90 Å, 3.14 Å, and 3.62 Å, with corresponding minima in σ^2 . This result is shown in Figure S3-1(a) of the supplementary material¹²⁸ and is entirely distinct from the cases for bromide and iodide (compare Figures S1-1 and S2-1 in the supplementary material).¹²⁸ Multiple distance minima strongly imply multiple solvation spheres, making chloride unique among the set of heavier halides.

The dependence of goodness-of-fit on CN showed a minimum at 6.5 oxygen scatterers (Figure S3-1(b) in the supplementary material).¹²⁸ However, consistent with the evidence for multiple shells, split shells always produced a better fit. For example, the one-shell CN = 6 model yielded Cl–O = 3.05 Å and weighted F = 0.1891, while the fit with two 3-oxygen shells yielded Cl–O = 2.92 Å (3O) and 3.13 Å (3O), weighted F = 0.1573, and F_M = 1.78 (Figures S3-2 and S3-3 in the supplementary material).¹²⁸

The two-shell fit could be further improved on addition of a single third oxygen scatterer at 3.62 Å (weighted F = 0.1073; F_M = 3.51 relative to the CN = 6 two shell fit), shown in Figure S3-4 in the supplementary material.¹²⁸ However, the three-shell model was set aside because of spline-induced systematic errors and the judgment that the EXAFS could not support an extended model. The EXAFS do support a divided solvation shell, however, with $4 \times \text{Cl–O} = 2.91$ Å and $3 \times \text{Cl–O} = 3.11$ Å. This fit appears in Figure 6 and the metrics are in Table V. The coordination number of

7 is in close agreement with the MXAN results (see below). The inverse CN = 7 two-shell fit with $3 \times \text{Cl–O} = 2.88$ Å and $4 \times \text{Cl–O} = 3.09$ Å was statistically indistinguishable (weighted F = 0.1539), but all other CN = 7 fits were of poorer quality. The homologous fit with $4 \times \text{Cl–O} = 2.87$ Å and $4 \times \text{Cl–O} = 3.09$ Å was also slightly poorer (weighted F = 0.1594; F_M = 0.93).

2. MXAN analysis

MXAN fits were judged acceptable when they reproduced the unusual double maximum of the XANES energy region (cf. Figure 1) that sets chloride apart from bromide and iodide. The fits were carried out independently of the information yielded by EXAFS, so that the first structural models included four, six, seven, and eight water molecules. In all cases, the starting symmetrical models became more disorganized during the course of the fit. These fits along with the initial and final structural models are shown in Figures S3-5 and S3-6, respectively, of the supplementary material.¹²⁸ The CN = 4 fit was very poor (goodness-of-fit $R_{sq} = 134.2$). The remaining models produced fits of $R_{sq} = 8.20$, 6.81, and 6.29, respectively. Figure S3-5 shows that these models did not reproduce the XANES or the continuum energy regions of the chloride K-edge XAS spectrum.

MXAN fits again showed that including 10 or more water molecules within hydrogen bonding distance of chloride risked unphysically close inter-water contacts. Additionally, neutron diffraction experiments had invariably found about 6-7 waters in the first solvation sphere of chloride.^{2,14,23} These results excluded structural models with highly populated first shells. Therefore, following the failure of the single-shell models, two-shell solvation models were constructed and tested. The previously obtained inner-shells of 6, 7, and 8 water molecules were retained, while the second shell water molecules were organized in a hydrogen-bonding array above the interstices between the first shell water molecules.

The results of these two-shell model MXAN fits, consisting of (first shell, second shell), CN = 6,7, CN = 7,7, and CN = 8,8 are displayed in Figure 7. In these fits, the first shell water molecules were fixed at their prior single-shell best-fit positions, and only the positions of the second shell water molecules were adjusted. The CN = 6 or CN = 8

TABLE V. EXAFS metrics for the chloride solvation sphere.

	[CN] R (Å) ^a	$\sigma^2 \times 10^3$	ΔE_0 (eV)	Weighted F
Cl–O	[4] 2.91 ± 0.01	23.95	−11.047	0.1537
Cl–O	[3] 3.11 ± 0.01	13.17		

^aCN is the coordination number. Uncertainty is the fit statistical e.s.d.; empirical uncertainty for room temperature solution EXAFS is of order ±0.03 Å. The σ^2 is in units of Å².

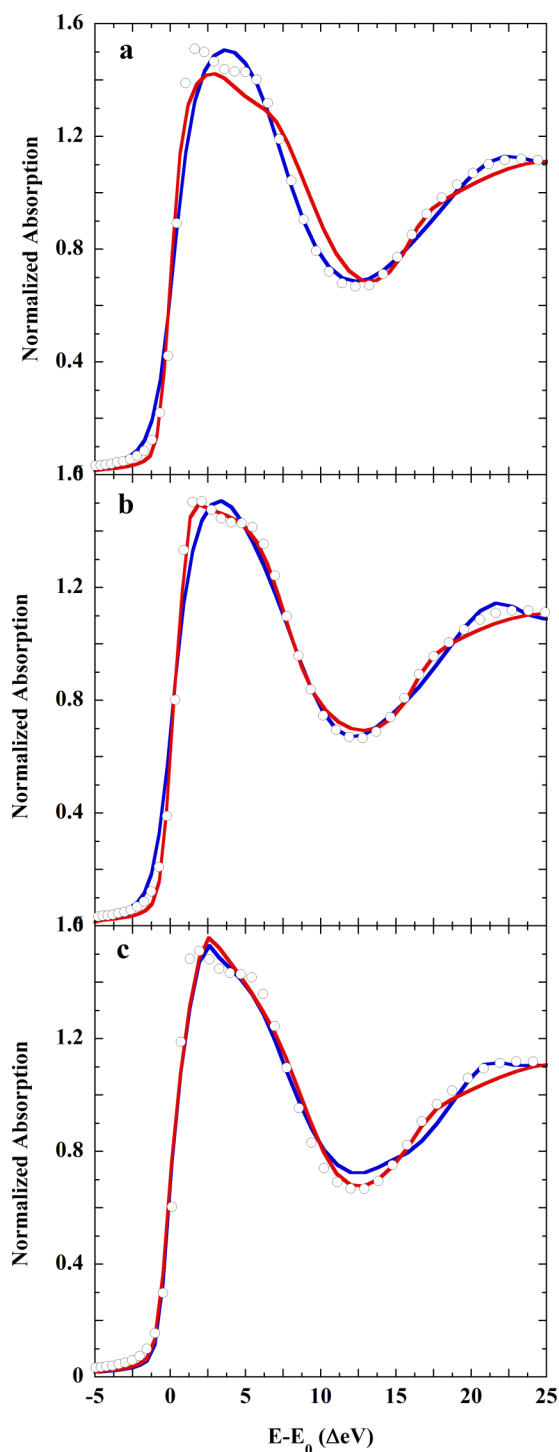


FIG. 7. (Open circle), the chloride K-edge XANES spectrum and the effect on the MXAN fit of sequential water molecule solvation shells. (a) (Blue solid line), six-water first shell and (red solid line), added seven-water second shell; (b) (blue solid line), seven-water first shell and (red solid line), added seven-water second shell; and (c) (blue solid line), eight-water first shell and (red solid line), added eight-water second shell. See also Figure S3-2 in the supplementary material.¹²⁸

second shell models did not improve the overall fit, showing $R_{sq} = 9.46$ and 6.18 , respectively. However, the fit was greatly improved when the seven-water second shell was added to the inner-shell $CN = 7$ structural model, producing $R_{sq} = 2.64$ (Figure 7(b)). In combination with a 7-water first shell, the

7-water second shell produced the correct intensity profile and double maximum of the XANES spectrum.

Adding a symmetrical eight-water second shell to the $CN = 8$ structural model did not improve the XANES spectrum and did not produce the double maximum (Figure 7(c)). However, Figure 7(a) shows that the seven-water second shell added to the $CN = 6$ structural model did produce the double maximum in the XANES spectrum, although the intensity was incorrect. Thus, this asymmetric seven-water second shell is necessary to the appearance of the double maximum on the rising K-edge.

The final MXAN analysis focused on the $CN = 7,7$ structural model (Figure 7(b)) and adjusted the positions of the first shell waters, with the second shell waters fixed at their prior best-fit positions. This fit produced a final goodness-of-fit $R_{sq} = 1.83$. The final two-shell model consists of an axially asymmetric array of water molecules, in a first shell $4 + 3$, second shell $4 + 3$ arrangement. The two shells also included an array of inter-shell hydrogen bonds that might stabilize such a structure in solution. The full XAS spectrum calculated for the 7,7 fit is shown in Figure S3-7 in the supplementary material,¹²⁸ and the metrics appear in Table VI.

Although the final two-shell solvation model produces a very good fit to the XAS spectrum, the specific $4 + 3/4 + 3$ arrangement may not be unique. For example, alternative structures, such as $3 + 4/4 + 3$ or $3 + 4/3 + 4$, were not explored. Nevertheless, two seven-water shells and axial asymmetry appear necessary to a description of chloride solvation.

D. Molecular dynamics

Reif and Hünenberger⁸⁸ developed the L_E , M_E , and H_E Lennard-Jones parameters for use in the molecular dynamics (MD) simulations of halide solvation. In a subsequent MD study, the L_E parameter produced Cl–O radial distributions that yielded a good correspondence with the chloride K-edge EXAFS spectrum.⁵³ In the present study, MD simulations of chloride solvation using the L_E , M_E , and H_E parameter produced D-MXAN R_{sq} error functions of 16, 23, and 107, respectively (Figures S4-1–S4-3 in the supplementary material).¹²⁸ The lower D-MXAN R_{sq} following the L_E parameter supports the previous EXAFS result. The L_E , M_E , and H_E parameters differ only in the magnitude of the L-J C_{12} interatomic repulsive parameter ($L_E = 126.2$, $M_E = 98.5$, and $H_E = 78.3$, each $\times 10^{-7}$ kJ mol⁻¹nm¹²).⁸⁸ It is therefore important to note that small changes in the L-J parameter can produce a large effect in the calculated XANES. Figure S4-4 shows the three respective Cl–O radial distribution functions (RDFs) calculated using MD.

Although the L_E version of the Lennard-Jones potential was best at reproducing the XAS spectrum, consistent with the results of Migliorati *et al.*,⁵³ the XANES region was incomplete (Figure S4-3 in the supplementary material).¹²⁸ This energy region is most sensitive to the geometry of the solvation sphere.

Further MD simulations using the GROMOS96 L-J parameters with the Encad-shift option, which reduces the Coulomb potential within the SPC/E water model, produced

TABLE VI. MXAN best fit metrics for the two chloride solvation spheres.

Shell	Cl-O (Å) ^{a,b}	Cl-H _{near} (Å) ^a	Cl-H _{far} (Å) ^a	Internal H-bond (shell) ^c
7 waters	3.15 ± 0.10	2.18 ± 0.10	3.50 ± 0.10	1.92 ± 0.04 Å (3 + 3)
7 waters	4.14 ± 0.31	3.76 ± 0.38	4.89 ± 0.30	2.0 ± 0.2 Å (4 + 4)
Prior work				
CN ^d	Cl-O (Å)	Cl-H _{near} (Å)	Method ^e	References
6 ± 1	3.1	2.2	ND,XRD	14
6.4 ± 0.3	3.1 ± 0.01	2.28 ± 0.03	ND	23
6.4	3.3	2.28	AXD	24
...	3.14 ± 0.02	...	SAXS	17
6.4	3.14 ± 0.02	2.23 ± 0.04	EXAFS	20

^aBond lengths include ±1σ scatter in Cl-L distance; L = O, H.^bThe Cl-O distance RMS ± (fit-error) ± (error standard deviation) was: first shell, ±0.28 ± 0.14 Å; second shell, ±0.36 ± 0.14 Å.^cThe average H-bond distance within each two-shell array.^dCoordination number.^eND, neutron diffraction; XRD, X-ray diffraction; AXD, anomalous X-ray diffraction; SAXS, small-angle X-ray scattering; EXAFS, extended X-ray absorption fine structure.

a slightly better average XAS spectrum of $R_{sq} = 14.3$ (Figure S4-5 in the supplementary material).¹²⁸ This result was further processed using the R_{th} criterion to obtain the simulated spectrum presented in Figure 8 (see Sec. II and Figure S4-6 and text in the supplementary material).¹²⁸

In Figure 8, the overall structure of the XAS spectrum is reproduced reasonably well. The XANES feature has nearly the correct intensity and width and is here better reproduced than in the H_E , M_E , or L_E simulations, or the full GROMOS96 simulation. The simulated XANES lacks the discrete double maximum found in the measured spectrum, but this energy region is highly sensitive to the structure of the second hydration shell (see Figure 7, and Figures S3-2 and S3-4 in the supplementary material).¹²⁸

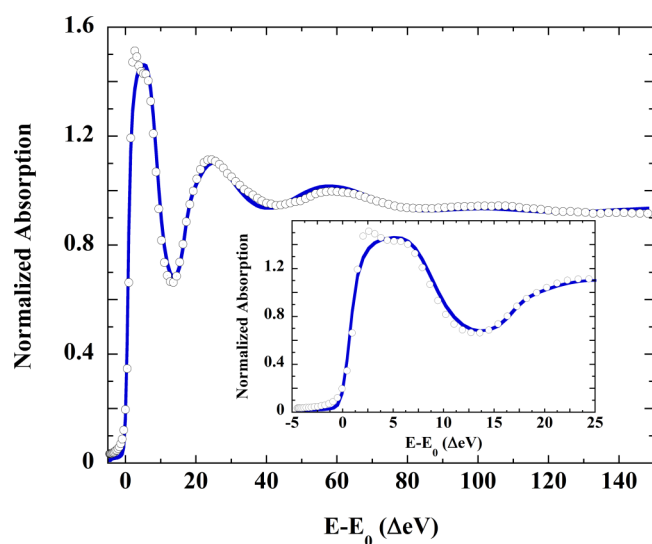


FIG. 8. (Open circle), K-edge XAS spectrum of dissolved chloride and (blue solid line), the spectrum calculated from the set of $R_{th} < 10^{-7}$ D-MXAN snapshots derived from the molecular dynamics simulation employing the GROMOS96 L-J parameters with the Encad-shift option and the SPC/E model, $R_{sq} = 7.1$ (see text). The R_{th} criterion selected 199 from the original 3190 frames in the simulation.

It is important to note here that an exact reproduction of the experimental XAS spectrum, which is the instantaneous average of a dynamic and approximately Gaussian redistribution of the hydration structure, is not expected from D-MXAN. Therefore, although the fit $R_{sq} = 7.1$ would not be considered good for an MXAN simulation, in which the structure is adjusted to minimize the R_{sq} value, the fact that there is broad agreement between experimental data and the MD simulated structure is promising. The filtered GROMOS96 D-MXAN simulation reproduced the intensities and approximate energies of the features at ~5 eV, 25 eV, 55 eV, and 100 eV, indicating that the predicted hydration shell is accurate to a first approximation (see Sec. IV for further details).

It is also clear that the refined GROMOS96 average is not equivalent to the fitted MXAN model because even this slightly more compressed structure does not quite reproduce the measured XANES spectrum. Nevertheless, the first shell RDF maximum of 3.14 Å is consistent with the MXAN structural model. The seven-water MXAN average first shell X-O distance of 3.15 ± 0.1 Å, implies a 3σ radial probability minimum near 3.45 Å, and the GROMOS96 integration indeed predicts 7.0 water molecules within this distance, though the first shell minimum occurs at 3.8 Å. However, the simulated second shell reaches the MXAN total of 14 water molecules at 4.8 Å, while the longest Cl-O second shell distance from the 14-water MXAN fit is 4.52 Å. The need for a further compression of the second hydration shell is thus indicated, highlighting a region of focus for improvement of theory. This effect is not easy to obtain with a two-body classical potential, because an alteration of the Cl-water or water-water interaction parameters would change the structure of the first hydration shell, as well. Nonetheless, the results show that the R_{th} model with the relatively low R_{sq} predicts the first shell average distance and number of water scatterers accurately.

The mean times of residence for a water molecule in the first or second shell were calculated using the method developed by Impey *et al.*⁹⁹ The calculation used the Gromos96 trajectory with the Encad function, as described in

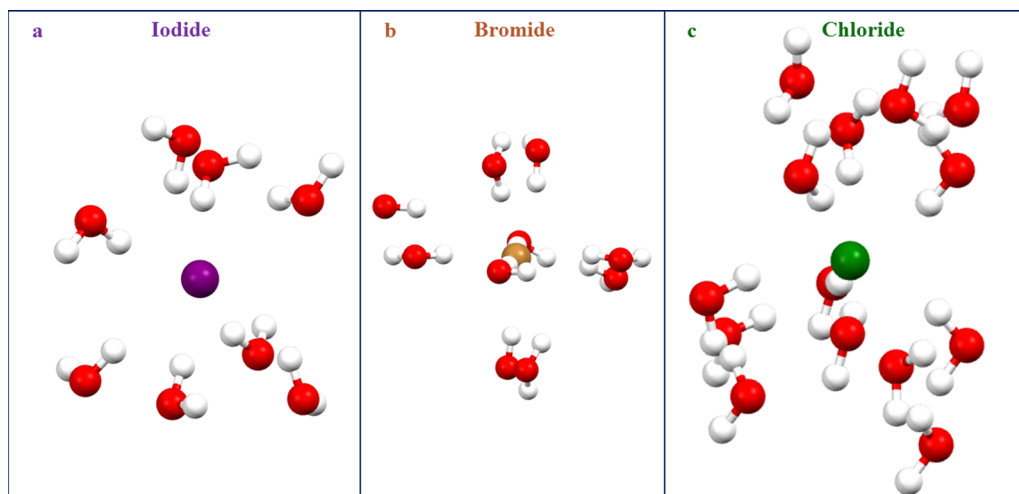


FIG. 9. MXAN structural models for dissolved aqueous, (a) iodide, (b) bromide, and (c) chloride. The supplementary material includes pdb files for full inspection of these structures.¹²⁸

Sec. II. The chloride first hydration shell was defined to be 0-3.7 Å, while the second was defined as 3.7-6 Å. Residence in a shell was defined as presence longer than 0.5 ps. The mean time of residence in the first shell was 4.8 ps. Second shell water molecules could translate either back into the first shell, or out into the bulk. The mean time between these transitions was 3.5 ps. The total chloride mean residence time of 6.6 ps relative to bulk is similar to the 7.6 ps calculated by Migliorati *et al.*,⁵³ and within the experimental residence time of 3-10 ps.¹⁰⁰

Finally, comparisons were made with MD simulations carried out using the AMBER potential in the SPC/E and TIP3P water models,^{84,101} as well as using the CHARMM potential with the SPC/E model, using the +ENCAD shift with the SPC/E model, or using the +ENCAD shift with the TIP5P model.^{85,102} Further, the OPLS potential was tested with the SPC/E water model.¹⁰³ A recent implementation of a polarizable potential in Gromacs was also tested,¹⁰⁴ using the Cl-OW Lennard-Jones parameters described in the work of Yu *et al.*,¹⁰⁵ and the SWM4-NDP water model.¹⁰⁶ The radial distribution functions resulting from these tests are shown in Figure S4-7 through Figure S4-10 in the supplementary material.¹²⁸

The D-MXAN calculation was then used to test all the MD simulations made with alternative potential schemes, against their ability to reproduce the XAS experimental spectrum. This showed that the various theoretical schemes yielded a reasonable reproduction of the continuum (EXAFS) energy region ($eV \geq 50$) of the chloride K-edge XAS spectrum, which is dominated by first shell single scattering and radial Cl-O distances. However, the calculated XANES spectra were significantly poorer in every case, relative to that found using the GROMOS96 potential already described. Thus, while the first shell radial distances were reasonable, the simulated solvation structures were not correct. These D-MXAN XAS spectra are shown in Figure S4-11 through Figure S4-14 of the supplementary material.¹²⁸ A set of $F = \sum_{i=1}^n (\chi_i^{\text{exp}} - \chi_i^{\text{MD}})^2 / N$ metrics ordering the simulation XANES spectra goodness-of-fit is given in Table S4-1 of the supplementary material.¹²⁸

E. Halide solvation models

The structural models derived from MXAN analysis are shown in Figure 9. In all structures, the immediate solvation shell waters are oriented with a hydrogen pointing toward the central halide. For chloride, the second shell water molecules are within hydrogen bonding distances of the first shell.

Room temperature K-edge XAS experiments measure the spectrum of each halide as it exists within a dynamical but evidently stable solvation structure (see below). These models best reproduce the measured XAS spectrum, and thus represent that equilibrium stable structure.

F. TD-DFT calculations

The near K-edge and rising K-edge XAS of the halides are strongly reflective of the ground state wave function. Thus a change in the ground state is expected to lead to a corresponding change in the valence electronic structure and hence in the near-edge spectrum. To test if changes in weak H-bonding solvent interactions can affect the near-edge XAS, TD-DFT was used to calculate the Cl 1s \rightarrow valence XAS transitions for three two-shell models with six-, seven-, and eight-water first shells, respectively. The results are presented in Figure 10, and show that the calculated spectra change dramatically with the immediate solvation structure.

These electronic state calculations show that despite negligible orbital overlap, the solvation sphere splits the chloride energy levels, leading to differences in the electronic part of the spectrum. This surprising result indicates that changes in the weak H-bonding water network about a halide ion can lead to dramatic changes in the valence molecular orbitals and therefore in the halide K-edge XAS spectra. Further, such changes occur with the entrance or exit of even a single water molecule. Overall, relatively small modifications of the solvation environment have a large impact on the halide electronic state. Thus the halide XANES spectrum is strongly sensitive to, and reflective of, the solvation structural details.

This implies that the XANES spectrum carries information about the solvation structural array, down to single-water

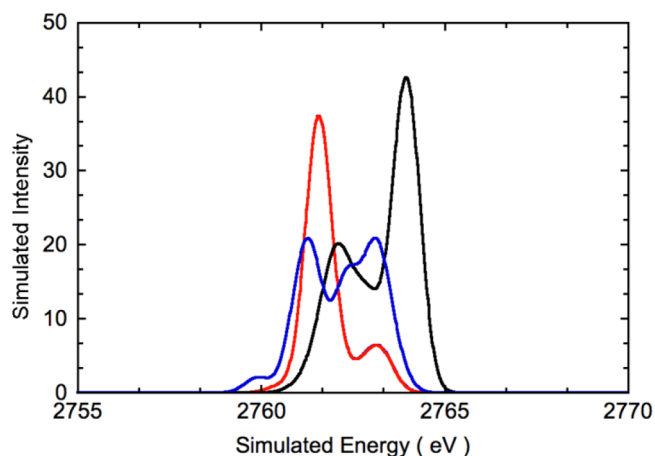


FIG. 10. TD-DFT simulated XAS spectra of the following: (blue solid line), 6-; (black solid line), 7-; and (red solid line), 8-coordinate first shell solvation models of chloride. A spectral broadening of 0.7 eV has been applied. The two-shell solvation spheres included a total of 13, 14, and 16 water molecules, respectively.

resolution. The shape of the XANES spectrum then strongly constrains the structural phase-space explored during an MXAN fit. The TD-DFT calculations show that the probability is very small that an incorrect structure will produce the correct XANES spectrum. Therefore the solvation models of Figure 9 are very likely close to the physically real solvation structures of the halides. A previous study of dissolved Ni(II) and Co(II) came to a similar conclusion about the impact of solvation structure on XANES spectra.¹⁰⁷

IV. DISCUSSION

Both the EXAFS and the MXAN fits demonstrate that the halides are solvated within discretely structured shells of water molecules. EXAFS analysis clearly showed that solvation of both bromide and iodide included only one shell of water molecules at a single average distance. In strong contrast, the chloride EXAFS implied water molecules in a divided solvation shell. These separate EXAFS structural classes are also indicated by the XANES spectra, in that bromide and iodide are similar while that of chloride is unique.

For all three halides, each solvation shell derived from MXAN analysis likely represents the average of a set of structurally cognate dynamical arrays of water molecules. The members of these dynamical arrays cannot depart too far from the modeled average, otherwise the XAS spectrum could not be closely reproduced by reference to a single structure. That is, the discrete MXAN analytical structures disconfirm the idea that halide solvation consists of multiple arrays of water molecules distributed among a wide range of coordination numbers, X–O distances, or O–X–O angles.

For example, radially disparate $X^- \cdots H-OH$ distances would severely reduce EXAFS intensity by the destructive interference of out-of-phase back-scattered photoelectron waves. To illustrate this point, Figure S5-1 in the supplementary material displays the variation in chloride K-edge EXAFS intensity with an increasing mean radial disorder of backscattering oxygen atoms.¹²⁸ The calculated

EXAFS intensity profile for the mean Cl–O displacement of ± 0.1 Å is generally consistent with the observed halide EXAFS intensity. Correspondingly, the mean scatter in X–O distance found by MXAN was also of order ± 0.1 Å ($X = Cl^-$, Br^- , I^-).

These results taken together indicate that water molecules are organized around chloride, bromide, and iodide in a globally coherent and persistent structural arrangement. In this circumstance, the dynamics involves rapid exchange with bulk water molecules but within a strongly bounded range of solvation number, of X–O distances, and of O–X–O angles. That is, the dynamical mechanism of water dissociation/association always yields the same general solvation structure, with only modest structural rearrangements overall. Gas-phase hydration energies for these halides, especially for chloride, also imply strongly H-bonded solvation spheres.^{108–110}

The discrete average structure at the center of a dynamical system represents the solvation ground state, which further includes the entire volume influenced by the halide. A net stabilization energy favoring one solvation structural array equivalent to half a water cluster hydrogen bond ($-\Delta G = 12$ kJ/mol)¹¹¹ yields a Boltzmann population ratio $N/N_0 = e^{(-\Delta G/RT)} = 124$ at 25 °C. That is, even a modestly favored structural array can achieve 99% dominance within a dynamical system. This array produced the observed EXAFS intensity, and is here revealed using MXAN analysis.

The aqueous solvation spheres of bromide and iodide are similar, while that of chloride is clearly in a class by itself. Chloride organizes the surrounding water molecules into two discrete structurally coherent but axially asymmetric shells. These shells are the foundational source of the unique XANES spectrum (cf. Figure 7). The XANES structure is further strictly dependent on the presence of axial asymmetry. The precise reason for the solvation asymmetry of chloride is obscure, because chloride is spherically symmetric. The polarizabilities of the two heavier halide ions are considerably greater than that of chloride,^{45,112} but the XAS of these latter ions did not support solvation asymmetry; nor was a two-shell structural model necessary to fit their XAS spectra. Thus polarizability is unlikely to be a source of the axial asymmetry in the solvation sphere of chloride.

Previous investigations of chloride solvation including neutron or X-ray scattering experiments,^{2,14–16,21,23,24} and molecular dynamics simulations,^{7,33,38,40,41,52,53,113} neither reported nor predicted an organized second solvation sphere for chloride. The small angle X-ray scattering and MD experiments of Bouzizi *et al.*¹⁷ are an exception, reporting two chloride hydration shells, with the first Cl–O = 3.22 Å but the second at a very distant 5.2 Å.

Nevertheless, it appears the MXAN two-shell chloride solvation model is consistent with the neutron diffraction (ND) radial distributions ($g(r)$).²³ Thus, for example, from the ND Cl–H_{1,1} = 2.28 Å (1,1 is inner hydrogen, inner shell), and using an average H–O = 0.95 Å and $\angle H-O-H = 105^\circ$, the average ND Cl–H_{1,2} distance (1,2 = inner shell, outer hydrogen) is 3.59 Å (cf. Figure S6-1 of the supplementary material).¹²⁸ The MXAN first shell Cl–H_{1,2} = 3.50 ± 0.10 Å is consistent with this ND result. The mean MXAN distance of Cl–H_{1,2} and Cl–H_{2,1} = 3.63 Å, which is very close to the

maximum of the second shell ND $g_{\text{Cl-H}}(r)$ (cf. Figure S6-1 of the supplementary material).¹²⁸ The first-shell 3.59 Å distance marks the forward edge of the maximum of the ND second solvation $g_{\text{Cl-H}}(r)$ feature, which tails away to a minimum at 4.44 Å. This 3.59–4.44 Å tail must imply hydrogens in further solvation shells.

Likewise, the MXAN second shell average $\text{Cl-O}_{2,1} = 4.14 \pm 0.31$ Å, and the second shell average $\text{Cl-H}_{2,1} = 3.76 \pm 0.38$ Å. The ND second $g_{\text{Cl-H}}(r)$ feature begins its steep descent at 3.76 Å (cf. the blue line in Figure S6-1 of the supplementary material).¹²⁸ Thus, the seven $\text{Cl-H}_{2,1}$ hydrogens are well within the neutron diffraction $g_{\text{Cl-H}}(r)$ distance envelope.

The mean MXAN second shell Cl-O distance = 4.14 Å, while the upper and lower bounds of this shell (3.6–4.5 Å) leave the ND first shell $g_{\text{Cl-O}}(r)$ intensity nearly untouched (cf. the green lines in Figure S6-1 of the supplementary material).¹²⁸ The area between these lines includes significant scattering intensity that can be assigned to the MXAN 7-water second shell. These will then reside at the inner edge of the larger ensemble of nearby water molecules detected by neutron diffraction. The XAS experimental result shows that the second solvation shell of chloride is more compact and well-organized than previously predicted. The continued rise of the ND $g_{\text{Cl-O}}(r)$ beyond 4.5 Å shows the nearby grouping of further water molecules within an extended field of chloride ion influence.

Car-Parrinello *ab initio* DFT/MD simulations of dissolved chloride have predicted an octahedral coordination sphere,^{48,50} or an asymmetric or disordered solvent array.^{7,53} For bromide and iodide, DFT/MD and QMMD simulations can predict unstructured solvation shells generally dominated by six water molecules, but with appreciable fractional populations with coordination numbers (CN) ranging from five to nine,^{35,53,114} or asymmetric solvation,^{7,8,54,115} or an ordered solvation shell.²¹ The variety of DFT/MD results recommends caution, and apparently reflects methodological reports of sensitivity to the choice of the specific basis set, and in some cases to the uncertainty in basis set superposition energy (BSSE) even with large basis sets.^{55,115}

The *R*th-filtered GROMOS96-based molecular dynamics simulation correctly predicted the coordination number and distance of the first chloride solvation shell (compare Figures 7 and 8). Only the structured second shell of chloride was missed within the filtered MD simulation. The EXAFS continuum energy region predicted using the various MD approaches is generally conformant with the measured spectrum. This higher energy correspondence is unsurprising because most of the EXAFS spectrum is determined by the radial distance of the first shell back-scatterers.

However, none of the tested MD force fields correctly reproduced the full chloride XAS spectrum. The greatest error was found within the XANES energy region, which is very sensitive to solvation structure. This implies that the simulated solvation spheres do not reflect physical reality and provides an opportunity to refine the force fields used in molecular dynamics. The set of MD frames obtained using the *R*th filter explore the limits of the MD simulation in reproduction of the experimental XANES signal. In the event, only about 6% of

the frames survived the filter. It seems likely that other MD simulations would fare similarly. This methodological focus indicates what can be learned by taking a sub-set of frames that better reproduce the experimental spectrum. The better agreement between experiment and theory produced by the *R*th frames (Figure 8) shows that a greater water density is required in the 3.1–5.0 Å range than is currently produced by theory. This result further shows that the structured second hydration shell is mandatory to obtain a good reproduction of the XANES. Modifications in theory to account for these observables will be required before these structures can emerge in MD simulations. In this light, it is significant that the best overall reproduction of the XANES spectrum was achieved by the MD simulation using the GROMOS96 L-J parameters with the Encad-shift option within the SPC/E water model.

Considerable literature discussion revolves about the impact of halide polarizability on the symmetry of bulk and interfacial solvation. Most molecular dynamics simulations that include halide polarization predict highly asymmetric, almost bowl-like, bulk solvation arrays,^{7,8,38,41,42,45,46,116,117} while others do not produce asymmetric solvation despite including halide polarization.³³ DFT QMMD simulations intrinsically include polarization, but apparently give mixed results.^{7,21,35,36,48,50,53,54,115}

MD simulations using a SPCE/POL polarization scheme show strictly surface solvation of chloride in 14- or 20-water clusters; equivalent to 2.5 m and 1.4 m solutions, respectively.^{41,116} Analogous MD simulations carried out using the TIP4P model produced interior solvation, implying surface solvation was not the result of an insufficiency of water molecules.¹¹⁶ These structures are highly similar to the external solvation predicted by gas-phase MD simulations of chloride in 6-water clusters.³⁸

In bulk water solution, strongly asymmetric solvation for chloride and iodide are predicted by the molecular dynamics simulations that include polarization, with a water large cavity to one side of the dissolved halide ion.⁴⁶ In this voided region, the average $\text{Cl} \cdots \text{H-OH}$ distance is 3.6 Å, well beyond the usual H-bonding range of 2.2–2.4 Å. For iodide the voided $\text{I} \cdots \text{H-OH}$ distance is 4 Å, compared to the typical 2.5 Å $\text{I} \cdots \text{H-OH}$ hydrogen-bonding distance. Similarly, theoretical calculations based in the AMOEBA force-field that also included anion polarization predicted asymmetric solvation structures about the halides in bulk water.^{8,117} The snapshots of bulk solvated chloride display an anisotropic structure interpreted as similar to asymmetric “surface-like” states.¹¹⁷ Such structures were also accepted as halide bulk solvation states by Knipping *et al.*¹¹⁸ and Lukyanov *et al.*¹¹⁹ The surface-solvated clusters from MD simulations noted above are all consistent with the asymmetric void-containing bulk solvation model of the halides. However, these asymmetric solvation states are not evident in the K-edge XAS of the dissolved halides.

To investigate this question further, a structural model of one of the proposed asymmetric chloride solvation spheres was constructed. The model was based on a stable solvation state predicted using molecular dynamics,³⁸ and implements the structural form of other proposed asymmetric bulk solvation models.^{41,44,45,116,118,120,121}

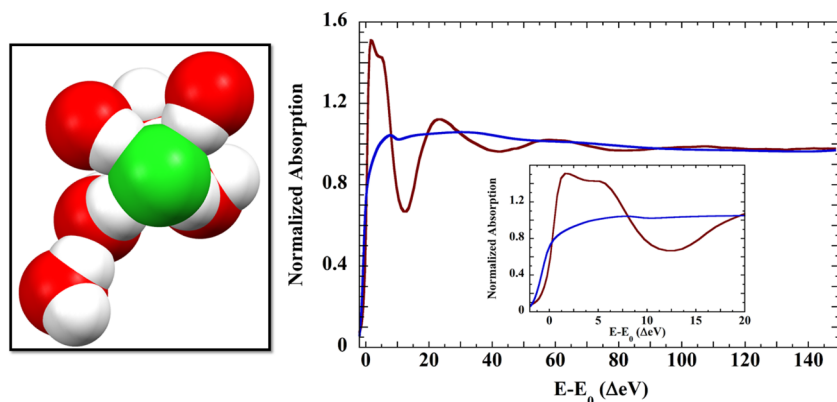


FIG. 11. The left panel shows the energy-minimized structural model for asymmetrically solvated chloride.³⁸ The right panel compares the chloride K-edge XAS spectra of (brown solid line), dissolved chloride as measured, and (blue solid line), the asymmetric structure, as calculated using MXAN; $R_{sq} = 151$.

The XAS spectrum of this structural model was then calculated using MXAN, and is compared with the measured spectrum in Figure 11. The severe mismatch conclusively demonstrates that in bulk solution, dissolved chloride includes no significant fraction of the asymmetric solvation proposed for surface chloride.¹ This conclusion is extended by the MD simulation using the Gromacs polarization potential, which also produced a severely mismatched XANES spectrum (cf. Figure S4-14 in the supplementary material).¹²⁸

Halide polarization is predicted to cause ion migration to, and a strongly preferred residence at, any air-water interface, e.g., that of suspended aerosol droplets.^{44,45,56–59,120,122–125} Greater polarization is predicted to produce greater surface concentrations. Thus, the polarization induced surface-enhanced solvation asymmetry of halides has been given an important role in the atmospheric chemistry of saline aerosols.^{1,118,120,122}

Halide polarization has been invoked to be both the source of asymmetric solvation in the bulk and the driving force for the enhancement of concentrations at air-water interfaces. Halide polarizability goes as $I^- > Br^- > Cl^-$,^{45,112} implying greater solvation asymmetry and greater enhancement of surface migration for the larger halides.^{8,46} However, the organized structures deduced here from K-edge XAS spectra do not support asymmetric halide solvation in bulk solution nor do they support theoretical formulations that predict an unstructured solvation sphere for dissolved chloride.^{52,117,126} The present results instead favor the theoretical models that predict organized and global solvation spheres in bulk water.^{8,33,47–49,127}

All the halides are homologous valence ns^2np^6 filled shell ions. Their respective K-edge XAS spectra should similarly be radically affected by a strongly asymmetric solvation structure. However, the solution XANES spectra of bromide and iodide do not show any sign of such asymmetry. The extreme mismatch between predicted and measured chloride XAS spectra is sufficiently profound as to eliminate such structures for dissolved bromide and iodide as well.

The present results will require revision of these associations. Polarization effects are not visible in the bulk solvation of the halides, even if the larger halides may polarize into solvation asymmetry upon arriving at an air-water interface. If the predicted asymmetries due to polarization do not appear in the solvation structures of the halides, then both excess migration to the surface

and any surface-enhanced halide concentration require a negative thermodynamic gradient with respect to the stable and symmetric solvation structures in bulk solution.

The structures derived here represent the first experimentally based three-dimensional aqueous solvation models for the halide ions most important to chemistry, biology, and geochemistry. Explicit solvation structural models can be used to quantitatively explore such diverse behaviors as solvation dynamics, the thermodynamics of electrode processes, the detailed mechanism of ion-pairing in solutions, in hydrous soils, and in aquifers, and halide ion interactions with proteins and nucleic acids. These experiment-based structures also emphasize the need to improve theoretical descriptions of solution structures and dynamics. Finally, the work reported here highlights the extraordinary resolving power of the combined EXAFS-MXAN methodology.

ACKNOWLEDGMENTS

This work was supported by Grant No. P41GM103393 (K.O.H.). Use of the Stanford Synchrotron Radiation Lightsource, SLAC National Accelerator Laboratory, is supported by the U.S. Department of Energy, Office of Science, Office of Basic Energy Sciences under Contract No. DE-AC02-76SF00515. The SSRL Structural Molecular Biology Program is supported by the DOE Office of Biological and Environmental Research and by the National Institutes of Health, National Institute of General Medical Sciences (including Grant No. P41GM103393). The contents of this publication are solely the responsibility of the authors and do not necessarily represent the official views of NIGMS or NIH.

¹T.-M. Chang and L. X. Dang, *Chem. Rev.* **106**, 1305 (2006).

²G. W. Neilson *et al.*, *Philos. Trans. R. Soc., A* **359**, 1575 (2001).

³W. H. Robertson and M. A. Johnson, *Annu. Rev. Phys. Chem.* **54**, 173 (2003).

⁴P. R. Smirnov, *Russ. J. Gen. Chem.* **83**, 1469 (2013).

⁵Y. Marcus, *Chem. Rev.* **109**, 1346 (2009).

⁶R. Tucceri, *Surf. Sci. Rep.* **56**, 85 (2004).

⁷L. Ge, L. Bernasconi, and P. Hunt, *Phys. Chem. Chem. Phys.* **15**, 13169 (2013).

⁸D. M. Rogers and T. L. Beck, *J. Chem. Phys.* **132**, 014505 (2010).

⁹W. Wachter *et al.*, *J. Phys. Chem. A* **109**, 8675 (2005).

¹⁰P. Westh *et al.*, *J. Phys. Chem. A* **110**, 2072 (2006).

¹¹I. Waluyo *et al.*, *J. Chem. Phys.* **140**, 244506 (2014).

¹²J. Boisson *et al.*, *Phys. Chem. Chem. Phys.* **13**, 19895 (2011).

¹³E. A. Raymond and G. L. Richmond, *J. Phys. Chem. B* **108**, 5051 (2004).

¹⁴A. H. Narten, F. Vaslow, and H. A. Levy, *J. Chem. Phys.* **58**, 5017 (1973).

¹⁵A. G. Sharpe, *J. Chem. Educ.* **67**, 309 (1990).

- ¹⁶M. D. Baer et al., *J. Phys. Chem. B* **118**, 7211 (2014).
- ¹⁷S. Bouazizi et al., *J. Phys. Chem. B* **110**, 23515 (2006).
- ¹⁸P. D'Angelo et al., *J. Chem. Phys.* **100**, 985 (1994).
- ¹⁹A. Filippini et al., *Chem. Phys. Lett.* **225**, 150 (1994).
- ²⁰J. L. Fulton and M. Balasubramanian, *J. Am. Chem. Soc.* **132**, 12597 (2010).
- ²¹J. L. Fulton et al., *J. Phys. Chem. B* **114**, 12926 (2010).
- ²²P. J. Merkling et al., *J. Chem. Phys.* **119**, 6647 (2003).
- ²³D. H. Powell, G. W. Neilson, and J. E. Enderby, *J. Phys.: Condens. Matter* **5**, 5723 (1993).
- ²⁴S. Ramos et al., *Chem. Phys.* **258**, 171 (2000).
- ²⁵H. Tanida, K.-i. Kato, and I. Watanabe, *Bull. Chem. Soc. Jpn.* **76**, 1735 (2003).
- ²⁶H. Tanida, H. Sakane, and I. Watanabe, *J. Chem. Soc., Dalton Trans.* **1994**, 2321.
- ²⁷H. Tanida and I. Watanabe, *Bull. Chem. Soc. Jpn.* **73**, 2747 (2000).
- ²⁸I. Watanabe and H. Tanida, *Anal. Sci.* **11**, 525 (1995).
- ²⁹V. Krishnan et al., *Z. Phys. Chem.* **218**, 1 (2004).
- ³⁰J. J. Rehr and R. C. Albers, *Rev. Mod. Phys.* **72**, 621 (2000).
- ³¹B. Santra et al., *Mol. Phys.* **113**, 2829 (2015).
- ³²J. R. Schmidt et al., *Chem. Phys.* **341**, 143 (2007).
- ³³M. Trumm et al., *J. Chem. Phys.* **136**, 044509 (2012).
- ³⁴E. Pluhařová et al., *Mol. Phys.* **112**, 1230 (2014).
- ³⁵P. D'Angelo, V. Migliorati, and L. Guidoni, *Inorg. Chem.* **49**, 4224 (2010).
- ³⁶A. P. Gaiduk et al., *Chem. Phys. Lett.* **604**, 89 (2014).
- ³⁷S. Raugei and M. L. Klein, *J. Chem. Phys.* **116**, 196 (2002).
- ³⁸D. J. Tobias, P. Jungwirth, and M. Parrinello, *J. Chem. Phys.* **114**, 7036 (2001).
- ³⁹J. VandeVondele et al., *J. Chem. Phys.* **122**, 014515 (2005).
- ⁴⁰G. Tóth, *J. Chem. Phys.* **105**, 5518 (1996).
- ⁴¹L. Perera and M. L. Berkowitz, *J. Chem. Phys.* **95**, 1954 (1991).
- ⁴²S. J. Stuart and B. J. Berne, *J. Phys. Chem.* **100**, 11934 (1996).
- ⁴³P. Jungwirth and D. J. Tobias, *J. Phys. Chem. B* **104**, 7702 (2000).
- ⁴⁴P. Jungwirth and D. J. Tobias, *Chem. Rev.* **106**, 1259 (2006).
- ⁴⁵P. Jungwirth and D. J. Tobias, *J. Phys. Chem. B* **106**, 6361 (2002).
- ⁴⁶C. D. Wick and S. S. Xantheas, *J. Phys. Chem. B* **113**, 4141 (2009).
- ⁴⁷J. E. Combariza, N. R. Kestner, and J. Jortner, *Chem. Phys. Lett.* **221**, 156 (1994).
- ⁴⁸J. M. Heuft and E. J. Meijer, *J. Chem. Phys.* **119**, 11788 (2003).
- ⁴⁹J. L. Fulton et al., *J. Chem. Phys.* **125**, 094507 (2006).
- ⁵⁰C. Zhang et al., *J. Chem. Phys.* **138**, 181102 (2013).
- ⁵¹L. X. Dang et al., *J. Phys. Chem. B* **110**, 23644 (2006).
- ⁵²A. Tongraar et al., *Phys. Chem. Chem. Phys.* **12**, 10876 (2010).
- ⁵³V. Migliorati et al., *J. Chem. Phys.* **141**, 044509 (2014).
- ⁵⁴V. T. Pham et al., *Chem. Phys.* **371**, 24 (2010).
- ⁵⁵B. Viswanathan, C. J. Barden, and R. J. Boyd, *Mol. Phys.* **104**, 389 (2006).
- ⁵⁶S. Ghosal et al., *Science* **307**, 563 (2005).
- ⁵⁷L. Piatkowski et al., *Nat. Commun.* **5**, 4083 (2014).
- ⁵⁸Y. Hirayama et al., *J. Phys. Chem. A* **115**, 8493 (2011).
- ⁵⁹M. Shoji et al., *J. Phys. Chem. A* **115**, 2148 (2011).
- ⁶⁰M. Benfatto, S. Della Longa, and P. D'Angelo, *AIP Conf. Proc.* **652**, 362 (2003).
- ⁶¹M. Benfatto, S. Della Longa, and P. D'Angelo, *Phys. Scr.* **2005**(T115), 28.
- ⁶²S. Della Longa et al., *Phys. Rev. Lett.* **87**, 155501 (2001).
- ⁶³C. R. Natoli et al., *J. Synchrotron Radiat.* **10**, 26 (2003).
- ⁶⁴J. Chaboy, M. Benfatto, and I. Davoli, *Phys. Rev. B* **52**, 10014 (1995).
- ⁶⁵M. Benfatto et al., *Biophys. Chem.* **110**, 191 (2004).
- ⁶⁶A. Zitolo and P. D'Angelo, *Chem. Phys. Lett.* **499**, 113 (2010).
- ⁶⁷P. Frank et al., *Inorg. Chem.* **47**, 4126 (2008).
- ⁶⁸P. Frank et al., *Inorg. Chem.* **51**, 2086 (2012).
- ⁶⁹P. Frank et al., *J. Chem. Phys.* **142**, 084310 (2015).
- ⁷⁰P. Frank et al., *Inorg. Chem.* **44**, 1922 (2005).
- ⁷¹E. Anxolabéhère-Mallart et al., *J. Am. Chem. Soc.* **123**, 5444 (2001).
- ⁷²R. Sarangi et al., *J. Chem. Phys.* **137**, 205103 (2012).
- ⁷³A. Tenderholt, B. Hedman, and K. O. Hodgson, in *X-ray Absorption Fine Structure-XAFS13*, edited by B. Hedman and P. Pianetta (American Institute of Physics, Stanford University, 2007), p. 105.
- ⁷⁴J. J. Rehr et al., *J. Am. Chem. Soc.* **113**, 5135 (1991).
- ⁷⁵S. I. Zabinsky et al., *Phys. Rev. B* **52**, 2995 (1995).
- ⁷⁶L. A. Bugaev et al., *Phys. Rev. B* **82**, 064204 (2010).
- ⁷⁷C. R. Natoli, M. Benfatto, and S. Doniach, *Phys. Rev. A* **34**, 4682 (1986).
- ⁷⁸M. Benfatto and S. Della Longa, *J. Phys.: Conf. Ser.* **190**, 012031 (2009).
- ⁷⁹A. Michalowicz et al., *J. Synchrotron Radiat.* **6**, 233 (1999).
- ⁸⁰E. A. Stern, *Phys. Rev. B* **48**, 9825 (1993).
- ⁸¹D. E. Sayers, "Error Reporting Recommendations: A Report of the Standards and Criteria Committee" (International X-ray Absorption Society, 2000), p. 1.
- ⁸²S. Pronk et al., *Bioinformatics* **29**, 845 (2013).
- ⁸³H. J. C. Berendsen, J. R. Grigera, and T. P. Straatsma, *J. Phys. Chem.* **91**, 6269 (1987).
- ⁸⁴W. L. Jorgensen et al., *J. Chem. Phys.* **79**, 926 (1983).
- ⁸⁵M. W. Mahoney and W. L. Jorgensen, *J. Chem. Phys.* **112**, 8910 (2000).
- ⁸⁶T. Darden, D. York, and L. Pedersen, *J. Chem. Phys.* **98**, 10089 (1993).
- ⁸⁷G. Bussi, D. Donadio, and M. Parrinello, *J. Chem. Phys.* **126**, 014101 (2007).
- ⁸⁸M. M. Reif and P. H. Hünenberger, *J. Chem. Phys.* **134**, 144104 (2011).
- ⁸⁹N. Schmid et al., *Eur. Biophys. J.* **40**, 843 (2011).
- ⁹⁰M. Levitt, *J. Mol. Biol.* **168**, 595 (1983).
- ⁹¹M. O. Krause and H. H. Oliver, *J. Phys. Chem. Ref. Data* **8**, 329 (1979).
- ⁹²M. Maeda and H. Ohtaki, *Bull. Chem. Soc. Jpn.* **48**, 3755 (1975).
- ⁹³A. K. Soper and K. Weckström, *Biophys. Chem.* **124**, 180 (2006).
- ⁹⁴J. E. Del Bene, *J. Phys. Chem.* **92**, 2874 (1988).
- ⁹⁵G. K. H. Madsen et al., *J. Phys. Chem. A* **103**, 8684 (1999).
- ⁹⁶T. Steiner, *Angew. Chem., Int. Ed.* **41**, 48 (2002).
- ⁹⁷A. Ranganathan, G. U. Kulkarni, and C. N. R. Rao, *J. Phys. Chem. A* **107**, 6073 (2003).
- ⁹⁸A. Filippini et al., *Phys. Rev. Lett.* **91**, 165505 (2003).
- ⁹⁹R. W. Impey, P. A. Madden, and I. R. McDonald, *J. Phys. Chem.* **87**, 5071 (1983).
- ¹⁰⁰P. Bopp, in *The Physics and Chemistry of Aqueous Ionic Solutions*, edited by M. C. Bellissent-Funel and G. W. Neilson (Springer, Netherlands, 1987), p. 217.
- ¹⁰¹A. E. Aliev et al., *Proteins* **82**, 195 (2014).
- ¹⁰²S. Piana, K. Lindorff-Larsen, and D. E. Shaw, *Biophys. J.* **100**, L47 (2011).
- ¹⁰³W. L. Jorgensen, D. S. Maxwell, and J. Tirado-Rives, *J. Am. Chem. Soc.* **118**, 11225 (1996).
- ¹⁰⁴J. A. Lemkul et al., *J. Comput. Chem.* **36**, 1473 (2015).
- ¹⁰⁵H. Yu et al., *J. Chem. Theory Comput.* **6**, 774 (2010).
- ¹⁰⁶P. T. Kiss and A. Baranyai, *J. Chem. Phys.* **137**, 194103 (2012).
- ¹⁰⁷M. Benfatto et al., *Phys. Rev. B* **56**, 2447 (1997).
- ¹⁰⁸M. Arshadi, R. Yamdagni, and P. Kebarle, *J. Phys. Chem.* **74**, 1475 (1970).
- ¹⁰⁹P. Kebarle, M. Arshadi, and J. Scarborough, *J. Chem. Phys.* **49**, 817 (1968).
- ¹¹⁰R. G. Keese and A. Castleman, *Chem. Phys. Lett.* **74**, 139 (1980).
- ¹¹¹Y. I. Neela, A. S. Mahadevi, and G. N. Sastry, *J. Phys. Chem. B* **114**, 17162 (2010).
- ¹¹²H. Coker, *J. Phys. Chem.* **80**, 2078 (1976).
- ¹¹³R. C. DeMille and V. Molinero, *J. Chem. Phys.* **131**, 034107 (2009).
- ¹¹⁴J. M. Heuft and E. J. Meijer, *J. Chem. Phys.* **123**, 094506 (2005).
- ¹¹⁵A. Ignaczak, J. A. N. F. Gomes, and M. N. D. S. Cordeiro, *Electrochim. Acta* **45**, 659 (1999).
- ¹¹⁶L. Perera and M. L. Berkowitz, *J. Chem. Phys.* **96**, 8288 (1992).
- ¹¹⁷Z. Zhao, D. M. Rogers, and T. L. Beck, *J. Chem. Phys.* **132**, 014502 (2010).
- ¹¹⁸E. M. Knipping et al., *Science* **288**, 301 (2000).
- ¹¹⁹S. I. Lukyanov, Z. S. Zidi, and S. V. Shevkunov, *J. Mol. Struct.: THEOCHEM* **725**, 191 (2005).
- ¹²⁰L. X. Dang, *J. Phys. Chem. B* **106**, 10388 (2002).
- ¹²¹L. X. Dang and T.-M. Chang, *J. Phys. Chem. B* **106**, 235 (2002).
- ¹²²P. Jungwirth and D. J. Tobias, *J. Phys. Chem. B* **105**, 10468 (2001).
- ¹²³D. H. Herce et al., *J. Chem. Phys.* **122**, 024513 (2005).
- ¹²⁴D. Horinek et al., *Chem. Phys. Lett.* **479**, 173 (2009).
- ¹²⁵C. Coleman et al., *Proc. Natl. Acad. Sci. U. S. A.* **108**, 6838 (2011).
- ¹²⁶S. G. Neogi and P. Chaudhury, *J. Comput. Chem.* **34**, 471 (2013).
- ¹²⁷J. E. Combariza, N. R. Kestner, and J. Jortner, *Chem. Phys. Lett.* **203**, 423 (1993).
- ¹²⁸See supplementary material at <http://dx.doi.org/10.1063/1.4959589> for information on (i) Normalized FT spectra of chloride, bromide, and iodide; (ii) EXAFS structural parameter search for iodide or bromide solvation; (iii) MXAN fits for bromide CN = 4, 6, 7, 8, or 10 water molecules; (iv) MXAN CN = 6 or 7 bromide solvation models; (v) EXAFS structural parameter search for chloride solvation; (vi) Cl K-edge EXAFS fit using 6, 7 (6,1), or 8 (6,1,1) oxygen scatterers; (vii) EXAFS metrics for homologous CN = 8 or 9 chloride models; (viii) EXAFS metrics for best CN = 7 or 8 chloride solvation models; (ix) MXAN CN = 6, 7, or 8 single shell fits to the chloride K-edge XAS; (x) MXAN CN = 6, 7, or 8 initial and final chloride single-shell models;

(xi) MXAN fit to chloride XAS employing the two-shell solvation model; (xii) MD structural XAS using the H_E , M_E , or L_E versions of the L-J potential; (xiii) Radial distribution and CNs of Cl–O for L_E , H_E , and M_E L-J Potentials; (xiv) MD structural XAS using the GROMOS96 L-J potential; (xv) MD GROMOS96 L-J Cl–O RDF after the R_{th} filter; (xvi) MD rdfs, AMBER potential, SPC/E and TIP3P water models; (xvii) MD rdfs CHARMM potential, SPC/E, +ENCAD, TIP5P water models; (xviii) MD rdfs OPLS, CHARMM, GROMOS96, and AMBER potentials; (xix) MD rdfs GROMOS96 and polarization potentials;

(xx) D-MXAN XANES from CHARMM potential and SPC/E water model; (xxi) D-MXAN XANES from CHARMM, +ENCAD shift and SPC/E; (xxii) D-MXAN XANES from CHARMM, +ENCAD shift and TIP5P; (xxiii) D-MXAN XANES from Gromacs polarization scheme; (xxiv) MD Scheme XANES Goodness of Fit; (xxv) EXAFS attenuation with mean back-scatterer displacement; (xxvi) Cl–H and Cl–O $g(r)$ s from neutron diffraction. PDB file of each of the three final halide XAS solvation models: chloride, Chloride_14_water.pdb; bromide, Bromide_8_water.pdb; and iodide, Iodide_8_water.pdb.